INTERNATIONAL JOURNAL FOR NUMERICAL METHODS IN ENGINEERING
Int. J. Numer. Meth. Engng 2004; **61**:716–737 (DOI: 10.1002/nme.1087)

A three-dimensional model describing stress-temperature induced solid phase transformations: thermomechanical coupling and hybrid composite applications

Ferdinando Auricchio[1,2,*,†] and Lorenza Petrini[1]

[1]*Dipartimento di Meccanica Strutturale, Università di Pavia, Via Ferrata 1, 27100 Pavia, Italy*
[2]*Istituto di Matematica Applicata e Tecnologie Informatiche, CNR, Via Ferrata 1, 27100 Pavia, Italy*

SUMMARY

Between composite materials, shape memory alloy (SMA) composites are having a more and more relevant role. Typically, SMA wires are embedded in a metallic or a polymeric matrix to obtain materials with native multi-functionality and adaptive properties. This work approaches the computational study of the mechanical response of a composite in which SMA wires, previously deformed, are activated by electrical current heating, and accordingly try to recover the original shape inducing a shape change or a prestress in the structure.

In particular, since the SMA behaviour is strongly affected by the thermo-mechanical coupling, in the first part of this work we present a 3D phenomenological model able to take into account this aspect. The model time-discrete counterpart is used to develop a 3D solid finite element able to describe the thermo-electro-mechanical coupled problem due to shape memory alloy response and to Joule effect. Finally, in the second part of the paper, we employ the developed computational tool to simulate different feasible SMA composite applications. Copyright © 2004 John Wiley & Sons, Ltd.

KEY WORDS: shape memory alloys; SMA hybrid composites; thermo-mechanical coupling; 3D constitutive model; boundary value problems

1. INTRODUCTION

Nowadays the behaviour of shape memory alloys (SMA) is quite well-known and effectively exploited; in fact, the use of such innovative materials has allowed the development of new devices and, at the same time, the enhancement of existing products [1–3]. Typically, the applications exploit the SMA capability to recover, once mechanically deformed, the original

*Correspondence to: Ferdinando Auricchio, Dipartimento di Meccanica Strutturale, Università di Pavia, Via Ferrata 1, 27100 Pavia, Italy.
†E-mail: auricchio@unipv.it

Contract/grant sponsor: Ministero dell'istruzione, dell'università e della ricerca (MIUR)

Received 6 August 2003
Published online 23 August 2004 *Revised 28 October 2003*
 Accepted 24 January 2004

shape through thermal loading (*shape memory effect*, *SME*) or through mechanical unloading (*pseudo-elasticity*, *PE*).

The peculiar SMA response depends on a thermo-elastic reversible transformation between two crystallographic structures with different physical and mechanical properties: the *austenite*, A, characterized by a more ordered unit cell and stable at temperatures above A_f (*martensite to austenite transformation finish temperature*), and the *martensite*, M, characterized by a less ordered unit cell and stable at temperatures below M_f (*austenite to martensite transformation finish temperature*) [4].

As a consequence, the *SME* is due to a temperature-driven transformation: when a specimen in the martensitic phase is loaded and unloaded at a temperature lower than M_f, it shows a non-linear response with a residual deformation; this residual (apparently inelastic) strain may be recovered (shape recovery) by heating the material above A_f, thus inducing a conversion of martensite into austenite. Finally, upon cooling the austenite is converted back into the original undeformed martensite. On the other hand, *PE* is due to a stress-driven transformation: when a specimen in the austenitic phase is loaded at a temperature greater than A_f, the material presents a non-linear behaviour due to a stress-induced conversion of austenite into martensite. Upon unloading, a reverse transformation from martensite to austenite occurs as a result of the instability of the martensite at zero stress for temperatures higher than A_f. At the end of the loading–unloading process no permanent strains are present and the stress–strain path is a closed hysteresis loop.

These two peculiar behaviours imply some interesting properties which allow to include SMA into the smart material category. Indeed, SMA sense mechanical, thermal or electrical stimuli and react with a designed response: for example, triggered by the reaching of a load or a temperature threshold, they can act recovering strain, inducing stress (when the shape recovery is constrained) or modifying the material properties. This aspect opens a new and probably even more interesting field of application: the realization of SMA-based smart hybrid composites [5–9].

Realized integrating smart materials into structures of different material, *hybrid composites* have native multi-functionality and adaptive properties: once connected to a control unit, they behave as *smart structures* able to respond to environmental changes in a pre-determinate manner [10]. Among the materials, which are commonly used to realize smart structures, SMA have recently received a lot of attentions [11]: in fact, SMA can be easily produced in several different shapes (from wires to porous bulk) and, once coupled with other materials, they show a good performance in tuning composite parameters, such as shape and stiffness, in response to environmental changes [12].

In most common applications SMA fibres are surface mounted or embedded in polymeric (thermoplastic or thermoset), metallic (Aluminium or Titanium) or plaster matrix and electrical current heating is used to induce thermally driven transformation.

Accordingly, hybrid composites with SMA have shown potential applicability in many fields: from medicine to aeronautics, from aerospatial to automotive field, from seismic to transportation engineering [13, 14]. In the following the most envisaged applications of SMA composite are briefly mentioned, in relation also to the SMA properties cited above.

1. *Active shape control*: In an hybrid composite with soft matrix and eccentrically posed SMA wires, shape changes may be induced through SME strain recovery. SMA wires or fibres in martensitic phase are prestrained and, successively, bounded on the surface or

embedded in the soft matrix; when heated they recover the original unstrained condition, inducing matrix deformation. Hence, a proper choice of wire position and heating time allow to control shape and position of the structure. A wide range of appliances employing this behaviour have been proposed, such as smart wings for airplanes [15], air management modules in climate control unit, smart space antenna reflectors [16], artificial muscles [17], large bending actuators [18].

2. *Active stress control*: In an hybrid composite with stiff matrix and centred or eccentrically posed SMA wires, prestress may be induced through SME constrained recovery. Prestrained martensitic wires are bounded on the surface or embedded in the stiff matrix in such a way that, when heated, they are prevented by the matrix from shrinking. As a consequence, they induce large stresses in the structure. It has been shown that this mechanism is useful for inducing prestress in concrete beams [19], for increasing resistance to traction and to fatigue crack propagation [20], for deformation reduction, damage control and self-repairing [21].
3. *Active vibration control*: In an hybrid composite embedded SMA wires may control the body mode shapes varying the stiffness of the structure [22]. This result can be reached inducing prestress in the structure through the constrained recovery of the martensitic wires [23–25] or exploiting the increment of the elastic modulus during the transformation from martensitic to austenitic phase [26, 27].
4. *Active impact resistance improvement*: In an hybrid composite embedded SMA wires may improve the low-impact resistance [28]. Indeed, when predeformed wires in austenitic phase are inserted into the structure, pseudo-elastic effect induces compressive stresses inhibiting cracking propagation and even promoting crack closure. On the other hand, the wires under impact-induced localized stresses undergo martensitic phase transformation, which allows them to achieve high strain levels and dissipate strain energy [29].

The cited examples suggest the important role that SMA hybrid composites can assume and the improvement that they can induce into technological developments. Moreover, the described applications highlight also the complexity of the composite behaviour due to the material interaction and the complex thermo-mechanical response of SMA.

In this frame numerical analyses may give an important support to design and optimize composites [30, 31]. With this aim, herein we propose a computational tool, investigating its ability to analyse and design the structural behaviour of SMA hybrid composites.

To describe the behaviour of SMA into the composite we use a 3D phenomenological model previously developed [32]. In particular, before approaching the hybrid composite study, we check the model capability to catch the characteristic thermo-mechanical SMA coupling. This aspect significantly influences the SMA response and, consequently, the global behaviour of SMA hybrid composites [33]. In literature, many of the proposed SMA constitutive models deal with the thermo-mechanical coupling, but only few authors approached its numerical implementation [34–41].

The present paper is organized as follows. In Section 2, starting from the constitutive equations of the model introduced in Reference [42], we derive the energy balance equation describing the heat exchange during phase transformation. Its discretized form is summarized and used to study coupled electro-thermo-mechanical problems. In particular, in Section 3 we check the developed algorithm through some simple electro-thermo-mechanical numerical tests. Finally, in Section 4 we approach the study of SMA hybrid composites: in the frame of the

finite element method we couple the 3D SMA model with a simple matrix constitutive model and we verify the overall computational tool solving different boundary value problems.

2. 3D PHENOMENOLOGICAL MODEL FOR SMA ELECTRO-THERMO-MECHANICAL COUPLING

The behaviour of SMA is characterized by a strong thermo-mechanical constitutive coupling due to the latent heat release or absorption during austenite–martensite phase transformations [43–47]. Hence, during the study of hybrid composites where the interaction between SMA and matrix may further increase the thermo-mechanical effect, a correct description of the mechanical response of SMA applications requires to take into consideration the thermo-mechanical coupling.

Accordingly, we investigate the ability of a previously presented model [42], in describing SMA thermo-mechanical coupling.

2.1. Time-continuous model

Following Reference [42], we assume the strain, $\boldsymbol{\varepsilon}$, split in its volumetric θ and deviatoric $\mathbf{e}$ components, and the absolute temperature, T, as control variables and the second-order transformation strain tensor, $\mathbf{e}^{\mathrm{tr}}$, as internal variable to characterize the thermodynamic state of an homogenized volume element. Moreover, we define the free energy function Ψ for a polycrystalline SMA in the following form:

$$\rho\Psi(\theta, \mathbf{e}, \mathbf{e}^{\mathrm{tr}}, T) = \frac{1}{2} K\theta^2 + G\|\mathbf{e} - \mathbf{e}^{\mathrm{tr}}\|^2 - 3\alpha K\theta(T - T_0) + \beta\langle(T - M_{\mathrm{f}})\rangle\|\mathbf{e}^{\mathrm{tr}}\| + \frac{1}{2} h\|\mathbf{e}^{\mathrm{tr}}\|^2 + (u_0 - T\eta_0) + c\left[(T - T_0) - T\ln\frac{T}{T_0}\right] + \mathscr{I}_{\varepsilon_{\mathrm{L}}}(\mathbf{e}^{\mathrm{tr}}) \tag{1}$$

where ρ is the material density, K is the bulk modulus, G the shear modulus, α the thermal expansion coefficient, T_0 a reference temperature, β the slope of the stress-temperature relation, M_{f} the martensite final transformation temperature, h the slope of the stress–strain relation during the stress-induced phase transformation, u_0 and η_0 the internal energy and the entropy at the reference state, respectively, c the heat capacity, $\langle\bullet\rangle$ the positive part of the argument, $\|\bullet\|$ the euclidean norm, $\mathscr{I}_{\varepsilon_{\mathrm{L}}}(\mathbf{e}^{\mathrm{tr}})$ the indicator function introduced to satisfy a constraint on the transformation strain norm and defined as:

$$\mathscr{I}_{\varepsilon_{\mathrm{L}}}(\mathbf{e}^{\mathrm{tr}}) = \begin{cases} 0 & \text{if } \|\mathbf{e}^{\mathrm{tr}}\| \leqslant \varepsilon_{\mathrm{L}} \\ +\infty & \text{if } \|\mathbf{e}^{\mathrm{tr}}\| > \varepsilon_{\mathrm{L}} \end{cases} \tag{2}$$

Following classical arguments [48], the first law of thermodynamics can be written as:

$$\rho\dot{u} = \rho(\dot{\Psi} + T\dot{\eta} + \dot{T}\eta) = \boldsymbol{\sigma} : \dot{\boldsymbol{\varepsilon}} + r - \nabla \cdot \boldsymbol{q} \tag{3}$$

where a superposed dot indicates variation in time, u and η are the current internal energy and entropy respectively, $\boldsymbol{\sigma}$ the Cauchy stress tensor, r the heat source, $\boldsymbol{q}$ the heat flux vector and ∇ the gradient operator.

Since hybrid SMA composites are often electrically activated by Joule effect, we extend the model to take into consideration a thermo-electro-mechanical coupling.

Limiting the discussion only to the steady-state, we recall that the electrical problem in an isotropic conductive material with an applied stationary potential difference is described by the following equations:

$$\begin{aligned} \nabla \cdot \boldsymbol{j} &= 0 \\ \boldsymbol{E} &= -\nabla V \\ \boldsymbol{j} &= \sigma^{\mathrm{el}} \boldsymbol{E} \end{aligned} \tag{4}$$

with $\boldsymbol{j}$ the current density, $\boldsymbol{E}$ the electric field, V the electric potential, σ^{el} the electric conductivity constant. Accordingly, between electrical and thermal fields, a coupling takes place through the Joule effect: when a current density $\boldsymbol{j}$ passes through a conductive body unit volume, the electric field $\boldsymbol{E}$ generates a power density in form of heating: $H_{\mathrm{elc}} = \boldsymbol{E} \cdot \boldsymbol{j}$.

Hence, under the hypotheses of small deformations, no internal heat source ($r = 0$), isotropic Fourier law ($\boldsymbol{q} = -K^{\mathrm{th}} \nabla T$, with K^{th} thermal conductivity constant), we can write the thermo-electro-mechanical coupled problem using the free energy definition (Equation (1)) into Equation (3), obtaining:

$$c\dot{T} - K^{\mathrm{th}} \Delta T = w'_{\mathrm{ch}} \tag{5}$$

where Δ is the Laplacian operator and w'_{ch} is the volume heat source defined as:

$$w'_{\mathrm{ch}} = H_{\mathrm{elc}} + D_{\mathrm{mec}} + H_{\mathrm{tmc}} \tag{6}$$

with H_{elc} the heat production due to the thermo-electrical coupling previously defined, D_{mec} the heat production due to the dissipative mechanical process, defined as:

$$D_{\mathrm{mec}} = \boldsymbol{\sigma} : \dot{\boldsymbol{\varepsilon}} - \rho \left(\frac{\partial \Psi}{\partial \theta} \dot{\theta} + \frac{\partial \Psi}{\partial \mathbf{e}} \dot{\mathbf{e}} + \frac{\partial \Psi}{\partial \mathbf{e}^{\mathrm{tr}}} \dot{\mathbf{e}}_{\mathrm{tr}} \right)$$

and H_{tmc} the heat production due to the thermo-mechanical coupling, given by the sum of the thermo-elastic effect and the phase transformation latent heat, defined as:

$$H_{\mathrm{tmc}} = \rho T \left(\frac{\partial \Psi}{\partial T \partial \theta} \dot{\theta} + \frac{\partial \Psi}{\partial T \partial \mathbf{e}} \dot{\mathbf{e}} + \frac{\partial \Psi}{\partial T \partial \mathbf{e}^{\mathrm{tr}}} \dot{\mathbf{e}}_{\mathrm{tr}} \right)$$

In particular, for the considered model it results:

$$\begin{aligned} D_{\mathrm{mec}} &= \mathbf{X} : \dot{\mathbf{e}}_{\mathrm{tr}} \\ H_{\mathrm{tmc}} &= \left(\beta \frac{\partial \|\mathbf{e}^{\mathrm{tr}}\|}{\partial \mathbf{e}^{\mathrm{tr}}} : \dot{\mathbf{e}}_{\mathrm{tr}} - 3K\alpha\dot{\theta} \right) T \end{aligned} \tag{7}$$

where the transformation stress $\mathbf{X}$ is the thermodynamic force associated to the transformation strain, defined as:

$$\mathbf{X} = -\rho \frac{\partial \psi}{\partial \mathbf{e}^{\mathrm{tr}}} = \mathbf{s} - \left[\langle \beta (T - M_{\mathrm{f}}) \rangle + h \|\mathbf{e}^{\mathrm{tr}}\| + \frac{\partial \mathscr{I}_{\varepsilon_{\mathrm{L}}}(\mathbf{e}^{\mathrm{tr}})}{\partial \|\mathbf{e}^{\mathrm{tr}}\|} \right] \frac{\partial \|\mathbf{e}^{\mathrm{tr}}\|}{\partial \mathbf{e}^{\mathrm{tr}}} \tag{8}$$

The model is completed introducing the following associate evolution law for $\mathbf{e}^{\mathrm{tr}}$:

$$\dot{\mathbf{e}}^{\mathrm{tr}} = \dot{\zeta}\,\frac{\partial F(\mathbf{X})}{\partial \boldsymbol{\sigma}} \tag{9}$$

with the Kuhn–Tucker conditions:

$$\dot{\zeta} \geqslant 0, \quad F \leqslant 0, \quad \dot{\zeta} F = 0$$

where F plays the role of limit function and $\dot{\zeta}$ plays the role of plastic consistent parameter. In particular, we assume the following yield function:

$$F(\mathbf{X}) = \sqrt{2J_2} + m\,\frac{J_3}{J_2} - R \tag{10}$$

where J_2 and J_3 are the second and the third invariant of the deviatoric tensor $\mathbf{X}$, defined, respectively, as:

$$J_2 = \tfrac{1}{2}\,(\mathbf{X}^2 : \mathbf{1}), \quad J_3 = \tfrac{1}{3}\,(\mathbf{X}^3 : \mathbf{1})$$

while R is the radius of the elastic domain in the deviatoric space, m is a material parameter. The parameters R and m can be related to the uniaxial critical stress in tension σ_{t} and in compression σ_{c} by the relation:

$$R = 2\sqrt{\frac{2}{3}}\,\frac{\sigma_{\mathrm{c}}\sigma_{\mathrm{t}}}{\sigma_{\mathrm{c}} + \sigma_{\mathrm{t}}}, \quad m = \sqrt{\frac{27}{2}}\,\frac{\sigma_{\mathrm{c}} - \sigma_{\mathrm{t}}}{\sigma_{\mathrm{c}} + \sigma_{\mathrm{t}}} \tag{11}$$

2.2. Time-discrete frame and solution algorithm

The time-discrete counterpart of the coupled electro-thermo-mechanical boundary value problem discussed in Section 2 is simply obtained focusing on a time interval $[t_n, t]$ with $t > t_n$ and using an implicit backward Euler formula to time integrate.

As example, indicating with the subscript n a quantity evaluated at time t_n and with no subscript a quantity evaluated at time t, the discrete form of the heat equation (5) is:

$$c\,\frac{T - T_n}{t - t_n} - K^{\mathrm{th}}\Delta T = \frac{1}{t - t_n}\Big[\mathbf{X} : (\mathbf{e}^{\mathrm{tr}} - \mathbf{e}^{\mathrm{tr}}_n) + T\beta\frac{\partial\overline{\|\mathbf{e}^{\mathrm{tr}}\|}}{\partial \mathbf{e}^{\mathrm{tr}}} : (\mathbf{e}^{\mathrm{tr}} - \mathbf{e}^{\mathrm{tr}}_n)$$
$$-3TK\alpha(\theta - \theta_n)\Big] + \sigma^{\mathrm{el}}\nabla V \cdot \nabla V \tag{12}$$

where for numerical purposes $\overline{\|\mathbf{e}^{\mathrm{tr}}\|}$ is a regularized norm [42] defined as:

$$\overline{\|\mathbf{e}^{\mathrm{tr}}\|} = \|\mathbf{e}^{\mathrm{tr}}\| - \frac{\delta^{(\delta+1)/\delta}}{\delta - 1}(\|\mathbf{e}^{\mathrm{tr}}\| + \delta)^{(\delta-1)/\delta}$$

with δ a smoothing parameter.

To solve the coupled electro-thermo-mechanical time-discrete problem (Equation (12)) we apply a partition technique, i.e we split the coupled problem in a sequence of uncoupled problems, searching for the global solution using an iterative procedure on the three partitions.

Skipping the electrical partition which is trivial, in the following we discuss the solution schemes adopted for the mechanical and thermal partitions.

2.2.1. Mechanical partition. Electrical and temperature fields are assumed fixed. Hence, as discussed in Reference [42] the mechanical field is computed after the solution of the following residual equations:

$$\begin{aligned} \mathbf{R}^X(\mathbf{X}, \Delta\zeta) &= \mathbf{X} - \mathbf{s}^{TR} + 2G\Delta\zeta \frac{\partial F}{\partial \boldsymbol{\sigma}} + [\langle \beta(T - M_f)\rangle + h\overline{\|\mathbf{e}^{tr}\|}] \frac{\partial \overline{\|\mathbf{e}^{tr}\|}}{\partial \mathbf{e}^{tr}} = \mathbf{0} \\ R^{\Delta\zeta}(\mathbf{X}, \Delta\zeta) &= F = \sqrt{2J_2} + m\frac{J_3}{J_2} - R = 0 \end{aligned} \tag{13}$$

where $\mathbf{s}^{TR} = 2G(\mathbf{e} - \mathbf{e}_n^{tr})$ is the trial stress defined in the frame of an elastic-predictor inelastic-corrector procedure; $\Delta\zeta$ is the discrete increment of the consistency parameter introduced to describe the transformation strain evolution rule as follows: $\mathbf{e}^{tr} = \mathbf{e}_n^{tr} + \Delta\zeta \partial F/\partial\boldsymbol{\sigma}$.

Adopting a Newton–Raphson method, from the linearization of Equation (13) we obtain:

$$\begin{aligned} \mathrm{d}\mathbf{R}^X(\mathbf{X}, \Delta\zeta) &= \mathbf{R}^X_{,\mathbf{X}} : \mathrm{d}\mathbf{X} + \mathbf{R}^X_{,\Delta\zeta}\, \mathrm{d}\Delta\zeta = \mathbf{0} \\ \mathrm{d}R^{\Delta\zeta}(\mathbf{X}, \Delta\zeta) &= \mathbf{R}^{\Delta\zeta}_{,\mathbf{X}} : \mathrm{d}\mathbf{X} + R^{\Delta\zeta}_{,\Delta\zeta}\, \mathrm{d}\Delta\zeta = 0 \end{aligned} \tag{14}$$

where the subscript comma indicates a derivative with respect to the quantity following the comma.

2.2.2. Thermal partition. Electrical and mechanical fields are assumed to be given. Hence, the temperature field is updated solving the heat equation written in residual form,

$$R(T) = c\frac{T - T_n}{t - t_n} - K^{th}\Delta T - (D_{mec} + H_{tmc} + H_{elc}) = 0 \tag{15}$$

Adopting a Newton–Raphson method the linearization of Equation (15) is trivial except for the following term:

$$\begin{aligned} \mathrm{d}(D_{mec} + H_{tmc} + H_{elc}) = \Bigg[& \mathrm{d}\mathbf{X} : (\mathbf{e}^{tr} - \mathbf{e}_n^{tr}) + \mathbf{X}\,\mathrm{d}\mathbf{e}^{tr} + T\beta \frac{\partial}{\partial \mathbf{e}^{tr}} \left(\frac{\partial \overline{\|\mathbf{e}^{tr}\|}}{\partial \mathbf{e}^{tr}} \right) \\ & : \mathrm{d}\mathbf{e}^{tr} : (\mathbf{e}^{tr} - \mathbf{e}_n^{tr}) + T\beta \frac{\partial \overline{\|\mathbf{e}^{tr}\|}}{\partial \mathbf{e}^{tr}} : \mathrm{d}\mathbf{e}^{tr} \\ & - 3\alpha K(\theta - \theta_n) + \beta \frac{\partial \overline{\|\mathbf{e}^{tr}\|}}{\partial \mathbf{e}^{tr}} : (\mathbf{e}^{tr} - \mathbf{e}_n^{tr}) \Bigg] \frac{1}{t - t_n} \end{aligned} \tag{16}$$

where the electrical contribution is null, being H_{elc} independent from the temperature. The term $\mathrm{d}\mathbf{e}^{tr}$ and $\mathrm{d}\mathbf{X}$ are calculated considering now Equation (13) as a function of the temperature as well as of the transformation stress and the consistency parameter at fixed strain. Accordingly,

from the linearized form of Equation (13):

$$\begin{aligned} \mathrm{d}\mathbf{R}^{X}(T,\mathbf{X},\Delta\zeta) &= \mathbf{R}^{X}_{,T}\,\mathrm{d}T + \mathbf{R}^{X}_{,\mathbf{X}} : \mathrm{d}\mathbf{X} + \mathbf{R}^{X}_{,\Delta\zeta}\,\mathrm{d}\Delta\zeta = \mathbf{0} \\ \mathrm{d}\mathbf{R}^{\Delta\zeta}(T,\mathbf{X},\Delta\zeta) &= R^{\Delta\zeta}_{,T}\,\mathrm{d}T + \mathbf{R}^{\Delta\zeta}_{,\mathbf{X}} : \mathrm{d}\mathbf{X} + R^{\Delta\zeta}_{,\Delta\zeta}\,\mathrm{d}\Delta\zeta = 0 \end{aligned} \tag{17}$$

with the coefficient $\mathbf{R}^{X}_{,X}$, $\mathbf{R}^{X}_{,\Delta\zeta}$, $\mathbf{R}^{\Delta\zeta}_{,X}$ and $\mathbf{R}^{\Delta\zeta}_{,\Delta\zeta}$ calculated during the mechanical partition solution and the derivative with respect to the temperature equal to:

$$\mathbf{R}^{X}_{,T} = \beta\frac{\partial\overline{\|\mathbf{e}^{\mathrm{tr}}\|}}{\partial\mathbf{e}^{\mathrm{tr}}}$$

$$R^{\Delta\zeta}{}_{,T} = 0$$

we obtain:

$$\begin{bmatrix} \mathrm{d}\mathbf{X} \\ \mathrm{d}\Delta\zeta \end{bmatrix} = -\begin{bmatrix} \mathbf{R}^{X}_{,X} & \mathbf{R}^{X}_{,\Delta\zeta} \\ \mathbf{R}^{\Delta\zeta}_{,X} & R^{\Delta\zeta}_{,\Delta\zeta} \end{bmatrix}^{-1}\begin{bmatrix} \beta\dfrac{\partial\overline{\|\mathbf{e}^{\mathrm{tr}}\|}}{\partial\mathbf{e}^{\mathrm{tr}}}\,\mathrm{d}T \\ 0 \end{bmatrix} \tag{18}$$

and

$$\mathrm{d}\mathbf{e}^{\mathrm{tr}} = \frac{\partial\mathbf{e}^{\mathrm{tr}}}{\partial\mathbf{X}}\,\mathrm{d}\mathbf{X} + \frac{\partial\mathbf{e}^{\mathrm{tr}}}{\partial\Delta\zeta}\,\mathrm{d}\Delta\zeta \tag{19}$$

where also $\partial\mathbf{e}^{\mathrm{tr}}/\partial\mathbf{X}$ and $\partial\mathbf{e}^{\mathrm{tr}}/\partial\Delta\zeta$ are known from the mechanical part. Substituting $\mathrm{d}\mathbf{e}^{\mathrm{tr}}$ and $\mathrm{d}\mathbf{X}$ into Equation (16), we can update the thermal field.

3. NUMERICAL EXAMPLES: ELECTRO-THERMO-MECHANICAL CONSTITUTIVE RESPONSE

We implement the procedure described in the previous section into the research oriented finite element code FEAP [49, 50]. Following a classical approach, we develop a thermo-electro-mechanical 3D eight-node brick element characterized by five degrees of freedom per node: the three components of displacement ($\boldsymbol{u}$), the temperature (T) and the electrical potential (V). We also develop a bi-dimensional element with one degree of freedom per node (the temperature T) to describe the thermal convection between the material and the surroundings through Newton's law [$q = h^{\mathrm{th}}(T - T_{\mathrm{ext}})$, with h^{th} convection parameter for unit area].

We start testing the developed computational tool effectiveness through the study of some simple homogeneous problems. In particular, for all the following examples we consider a SMA specimen with a length of 10 mm, a rectangular cross-section of 1×1 mm and the external faces covered by the bi-dimensional elements for convection.

3.1. Thermo-mechanical coupling

We refer to the work of Lim and McDowell [47] to define the first set of numerical tests and to deduce reliable material parameters, however without adopting any systematic identification

Table I. Numerical tests: shape-memory-alloy material properties.

Parameters	SMA 1	SMA 2	SMA 3
Young modulus E (MPa)	120 000	120 000	70 500
Hardening h (MPa)	1500	1500	3400
Comp. critical stress σ_c (MPa)	72	137	140
Tens. critical stress σ_t (MPa)	56	110	140
Poisson modulus ν (dimensionless)	0.3	0.3	0.3
Limit strain ε_L (dimensionless)	0.04	0.04	0.07
Stress/temp. param. β (MPa/K)	6	2	4.45
Thermal exp. coef. α (1/K)	1.E-6	1.E-6	1.E-6
Thermal conduct. K^{th} (W/(m K))	18	18	18
Heat capacity c (J/(cm^3 K))	5.44	5.44	2.05
Elettr. conduct. σ^{el} (1/(Ω cm))	12 000	12 000	12 000
Mart. finish trans. temp. M_f (K)	218	218	241
Mart. initial trans. temp. M_s (K)	240	240	250
Aust. initial trans. temp. A_s (K)	253	253	265
Aust. finish trans. temp. A_f (K)	273	273	273

procedure. Indeed, our aim is not to reproduce exactly the cited experimental results, but to illustrate the performance of the proposed constitutive model.

The SMA material properties considered in this problem are reported in Table I in the column indicated as 'SMA 1'. Moreover we set the initial body temperature and the reference temperature equal to 293 K, i.e. above A_f; we assume the heat convection parameter $h^{th} = 1.5\,\mathrm{J/(m^2\,K)}$ and the smoothing parameter $\delta = 0.02$.

Among the several numerical analyses performed, herein we present the results of a tension–compression cyclic test performed imposing the following strain history:

Step	Cycles	Strain path	Strain rate
1	1–5	$\pm 3\%$	$5 \times 10^{-4}\ \mathrm{s}^{-1}$
2	6	$\pm 3\%$	$5 \times 10^{-6}\ \mathrm{s}^{-1}$

Figures 1(a) and 1(b) compare the responses of the six cycles in terms of stress–strain and strain-temperature, respectively. The results qualitatively agree with the experimental results [47], showing the peculiarities of the typical pseudo-elastic response ($T_{test} > A_f$). In the first 5 cycles, the model response is such that:

- during loading (both tension and compression) the transformation from austenite to single variant martensite takes place with latent heat release and hence with specimen heating
- during unloading (both tension and compression) the transformation from single variant martensite to austenite takes place with latent heat absorption and hence with specimen cooling
- during the cycles, the thermal balance between the specimen and the surrounding is such that the heat can be transferred out of the specimen, and hence the entire stress–strain profile shifts down. Accordingly, the transformation stress at the first cycle is higher than the others

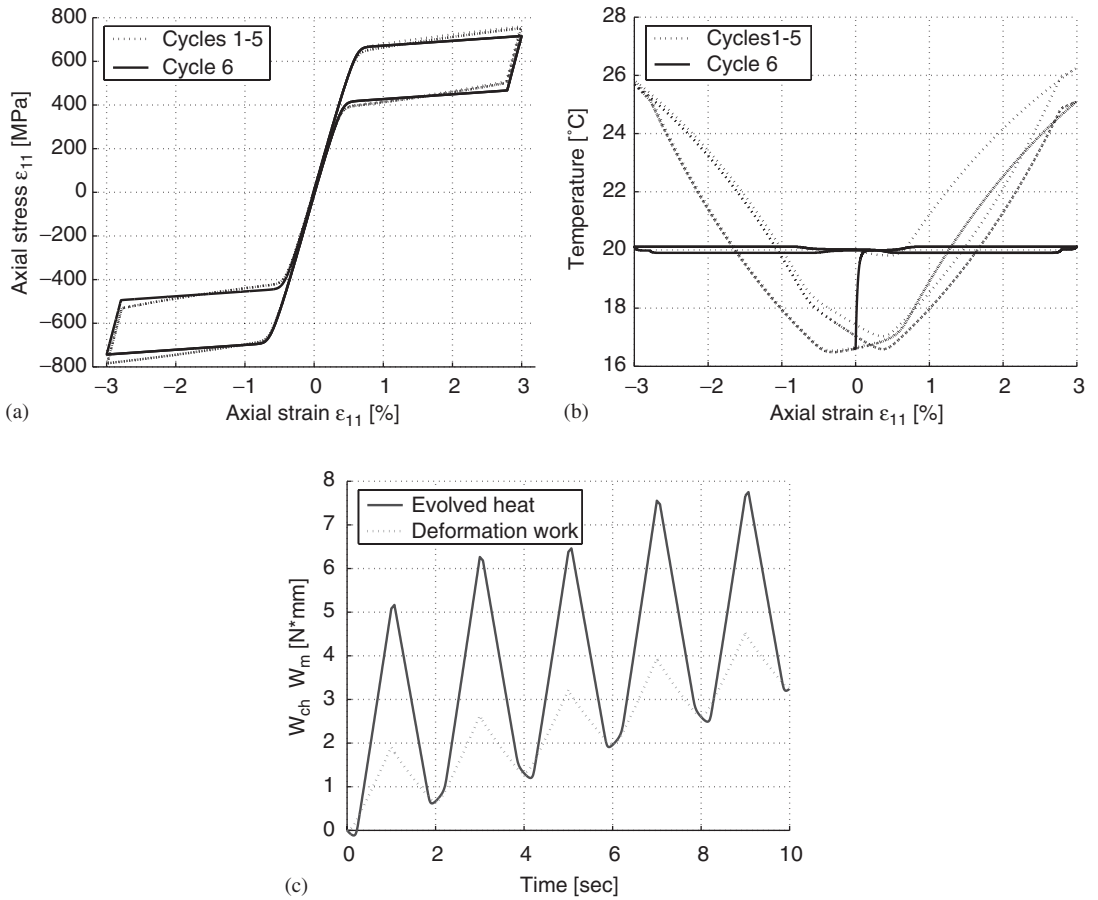

Figure 1. SMA specimen response under cyclic tension–compression test at different strain rates: $5 \times 10^{-4}\,s^{-1}$ in the first 5 cycles, $5 \times 10^{-6}\,s^{-1}$ in the last cycle. Comparison between the stress–strain curves (a) and the temperature–strain curves (b) of the 6 cycles. Comparison between the evolved heat and the deformation work during the first 2 cycles and half (c).

Moreover, the model is able to describe the effects associate to a strain rate variation. In particular during the sixth cycle we reduce the strain rate of two order of magnitude in comparison with the previous cycles, and we notice that:

- the heat has the time to flow out by convection, maintaining the specimen temperature almost constant during phase transition
- the slope of the stress–strain curve during the phase transition decreases, at the limit overlapping to a purely mechanical response (not reported in the figure).

To make more clear the model thermo-mechanical behaviour, in Figure 1(c) we compare the cyclic variation of the deformation work W_m and the evolved heat W_{ch} [51],

defined as:

$$W_m = V_0 \int_0^t (\boldsymbol{\sigma} : \dot{\boldsymbol{\varepsilon}})\, \mathrm{d}\tau$$
$$W_{\mathrm{ch}} = V_0 \int_0^t \left(\mathbf{X} : \dot{\mathbf{e}}^{\mathrm{tr}} + \beta \frac{\partial \|\mathbf{e}^{\mathrm{tr}}\|}{\partial \mathbf{e}^{\mathrm{tr}}} : \dot{\mathbf{e}}^{\mathrm{tr}} - 3K\alpha\dot{\theta} \right) \mathrm{d}\tau \tag{20}$$

where V_0 is the specimen volume. At each cycle, there is an amount of released energy which is not recovered, hence both the two curves show a positive trend: it means that the model is intrinsically dissipative [35]. In particular, the hysteresis loop amplitude depends on the intrinsic dissipated energy (D_{mec}) being strongly related to the magnitude of the thermodynamic force $\mathbf{X}$.

3.2. Electro-thermo-mechanical coupling

In this problem the heating power generated by electrical current is exploited to induce temperature-driven transformation into the specimen and, accordingly, to recover the original undeformed shape, once removed the load. The SMA material properties considered are reported in Table I in the column indicated as 'SMA 2'. Moreover we set the initial body temperature and the reference temperature equal to $M_{\mathrm{f}} = 218\,\mathrm{K}$; we assume the heat convection parameter $h^{\mathrm{th}} = 0.15\,\mathrm{J/(m^2\,K)}$ and the smoothing parameter $\delta = 0.02$.

Among the several numerical analyses performed, herein we present the results of a uniaxial test performed imposing the following force and electric potential history:

Step	Load type	Path	Time (s)
1	Force	0–80 MPa	0–4
2	Force	80–0 MPa	4–8
3	Pot. difference	0–3 V	8–9
4	Pot. difference	3 V	9–14
5	Pot. difference	3–0 V	14–15

The test results are summarized in Figure 2. In particular Figure 2(a) shows the classical stress–strain curve of the material in martensitic phase, with a residual strain of 3.3% after unloading and its recovery at zero stress after heating (dotted line). Looking at the temperature-time curve (Figure 2(b)), we notice a temperature increment of about 3°C between 1.3 and 2.3 s, due to the transformation latent heat: in the same time interval the transformation strain increases from zero to the maximum. After 8 s, the electric potential difference applied at the edges of the specimen (Figure 2(c)) induce the temperature to increase above A_{f}. Accordingly, the transformation strain is recovered (Figure 2(d)).

The presented results and the optimal convergence of the algorithm indicate the efficiency of the model to describe the electro-thermo-mechanical coupling behaviour of SMA.

4. NUMERICAL EXAMPLES: HYBRID COMPOSITES

As underlined in Section 1, one of the more interesting and promising way to employ SMA is in composite production: indeed, the fields of potential applications for the SMA hybrid composites are enormous.

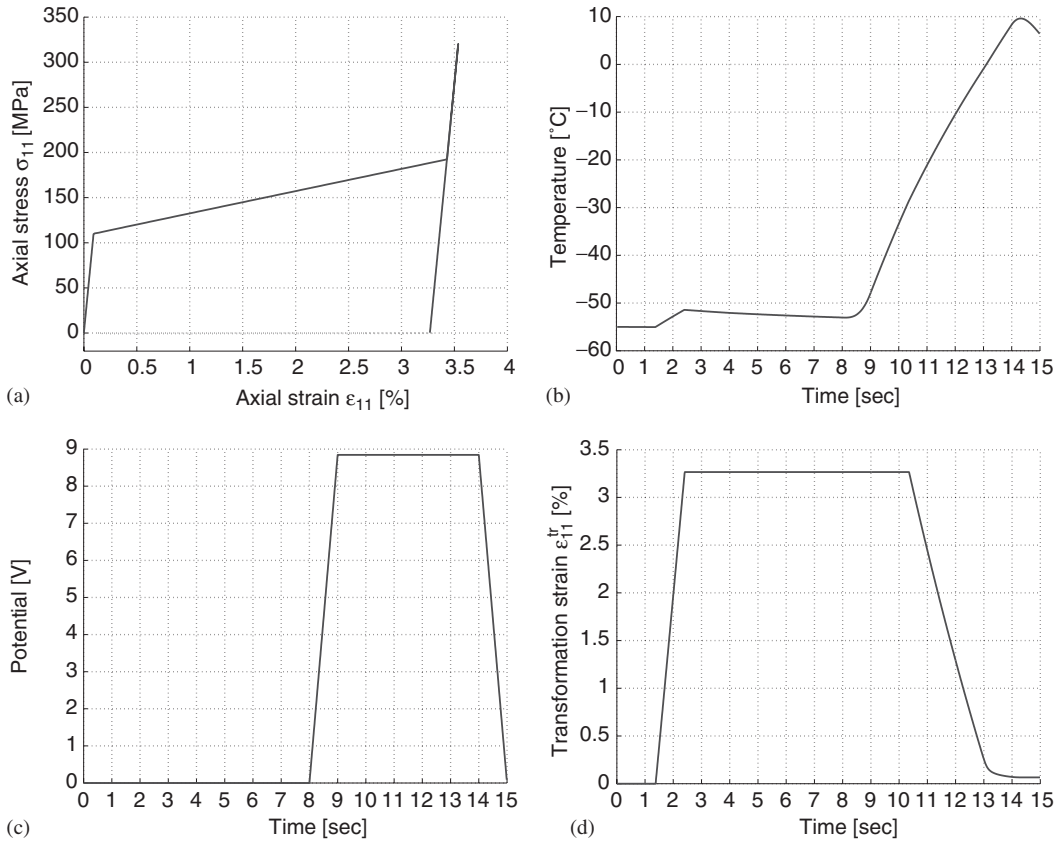

Figure 2. SMA specimen response under mechanical and electrical stimuli. Stress–strain curve during loading–unloading at temperature lower than M_f (continuous line) and during heating above A_f (dotted line) (a), temperature (b), potential difference (c) and transformation strain (d) time history.

Up to now, in our knowledge, a big effort has been devoted to investigate experimentally the behaviour of always new invented composites [52–54], while only few researchers tried to predict numerically the experimental response and to design new devices. Among them, Venkatesh *et al*. [27] use a simple beam finite element to predict active vibration control possibilities for planar mechanisms with Ni–Ti reinforced composite; Thompson *et al*. [55] use standard finite element analysis to investigate the active buckling control of stiffened panels by embedded SMA rods; Ro *et al*. [56] propose a finite element model to study the static and dynamic characteristics of Ni–Ti-reinforced composite plates; Hurlbut *et al*. [57] implement a 3D SMA constitutive model within a shell based finite element code and study a passive vibration isolator; Benzaoui *et al*. [58] study experimentally and numerically the behaviour of a basic actuator consisting in a single Ni–Ti SMA wire loaded by a mass; de Blonk *et al*. [59] model the deflection of a flexible rod with embedded two way shape memory actuators; Lagoudas *et al*. [60] model a thermoelectrically cooled thin SMA layer extensional actuator; Ostachowicz *et al*. [61] present finite element governing equations and solution procedures to study natural frequencies of SMA fibre-reinforced composite plate; Su *et al*. [62] propose a

2D constitutive model for a SMA reinforced composite laminated plate; Baz *et al*. [63] study experimentally and numerically the shape control of a SMA reinforced composite beam through SMA strips thermally trained to provide and memorize controlled transverse deflections; Lau *et al*. [64] present an analytical model for the evaluation of natural frequencies of glass fibre composite beams with embedded SMA wires. These works suggest that a properly developed computational tool can be useful to support the design of advanced hybrid composites exploiting the SMA features.

Accordingly, in the last part of this work we investigate the possibility to study through the finite element method the behaviour of an hybrid composite, coupling the 3D thermo-electro-mechanical model previously described with a simple constitutive model of the matrix.

Finally, we retain that our approach may offer some advantages with respect to some of the previously cited models:

- The SMA behaviour is described by a 3D model; accordingly, composite with SMA element of generic shape can be studied.
- The model joins accuracy and simplicity in describing SMA peculiar response; accordingly it can be usefully implemented in different finite element codes.
- The composite is described distinguishing between SMA elements and matrix; accordingly it allows to catch the interaction between the two parts and hence the effect of SMA thermo-mechanical coupling.
- The developed computational tool is efficient and robust.

4.1. Boundary value problems

We verify the computational tool capability through the study of four different applications, exploiting either active shape control or active stress control.

In the four boundary value problems, we consider Nickel–Titanium wires embedded in or surface mounted on matrices of different materials (Aluminium, soft and stiff polymers). The bi-dimensional elements for convection cover the composite external faces.

In particular, the Nickel–Titanium wires are described by the presented model using the material parameters summarized in column 'SMA 3' of Table I. Moreover we assume the smoothing parameter $\delta = 0.02$. The Aluminium matrix is described either by an elastic or elasto-plastic model with hardening, while the stiff and soft polymeric matrices are described by an elastic model. All the material parameters are reported in Table II. Finally, the bi-dimensional elements are characterized by the convection parameter $h^{\text{th}} = 0.1\,\text{J}/(\text{m}^2\,\text{K})$.

4.1.1. Problem A. Referring to the numerical tests performed by Aboudi [65] we consider the case of a composite (dimension $10 \times 1 \times 4$ mm) with an Aluminium matrix, reinforced by Nickel–Titanium wires in austenitic phase and oriented in the x_1 direction: we assume the SMA wires concentrated in two layers (Figure 3—left part), with volume fraction of $v_w = 0.3$.

We perform uniaxial loading-unloading tests in the x_1 direction under displacement control both on the reinforced ($v_w = 0.3$) and on the unreinforced matrix ($v_w = 0$). Moreover, the reinforced composite behaviour is studied considering two cases: perfectly elastic and elasto-plastic matrix response.

Room and body initial temperatures are set at $344\,\text{K} > A_\text{f}$. Moreover the chosen test strain rate and convection parameter allow the body temperature to remain constant during all the test.

Table II. Numerical tests: hybrid composite matrix material properties.

Parameters	Alumin. matrix	Stiff pol. matrix	Soft pol. matrix
Young modulus E (MPa)	72 400	36 000	3600
Kinem. hardening h_k (MPa)	5000		
Yielding stress σ_y (MPa)	300		
Poisson modulus v (dimensionless)	0.33	0.305	0.305
Thermal exp. coef. α (1/K)	1.0E-6	6.4E-6	6.4E-6
Thermal conduct. K^{th} (W/(m K))	190	1.E-7	1.E-7
Heat capacity c (J/(cm^3 K))	2.4	5.0	5.0
Elettr. conduct. σ^{el} (1/(Ω cm))	200 000	1.E-14	1.E-14

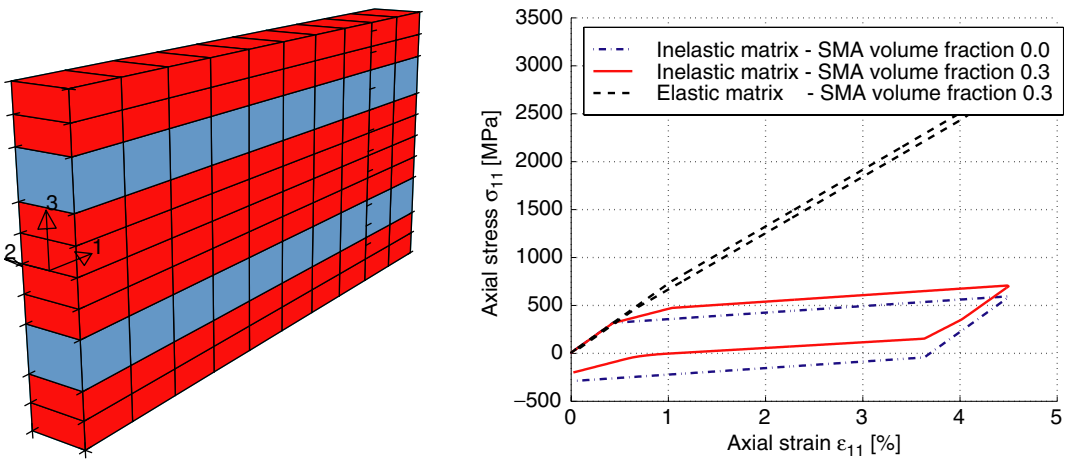

Figure 3. Model of hybrid composite with austenitic SMA wires (volume fraction $v_w = 0.3$) embedded in Aluminium matrix (Problem A) (left part). Axial response comparison between hybrid SMA-Al composite with perfectly elastic matrix, SMA-Al composite with elasto-plastic matrix and Aluminium elasto-plastic matrix without SMA wires (right part).

The right part of Figure 3 presents the results in terms of axial stress and strain average values which are in good agreement with the results presented by Aboudi [65].

4.1.2. Problem B. We investigate the performance of the proposed computational tool in simulating the shape control induced by strain recovery (*active shape control*). In particular, we consider a composite beam (dimension $10 \times 2 \times 1$ mm) with two Ni–Ti prestrained wires in martensitic phase, with volume fraction $v_w = 0.125$, surface mounted on a soft polymeric matrix, along the x_1 direction (Figure 4(a)). Room and body initial temperatures are set at 241 K $= M_f$.

Prestrained SMA wires are alternatively activated by heating (Figure 4(b)). We start imposing a potential difference of 4 V at the edges of the upper wire (Figure 4(c)): the wire heats above A_f and tends to shrink inducing controlled beam bending; in the studied case the tip of the

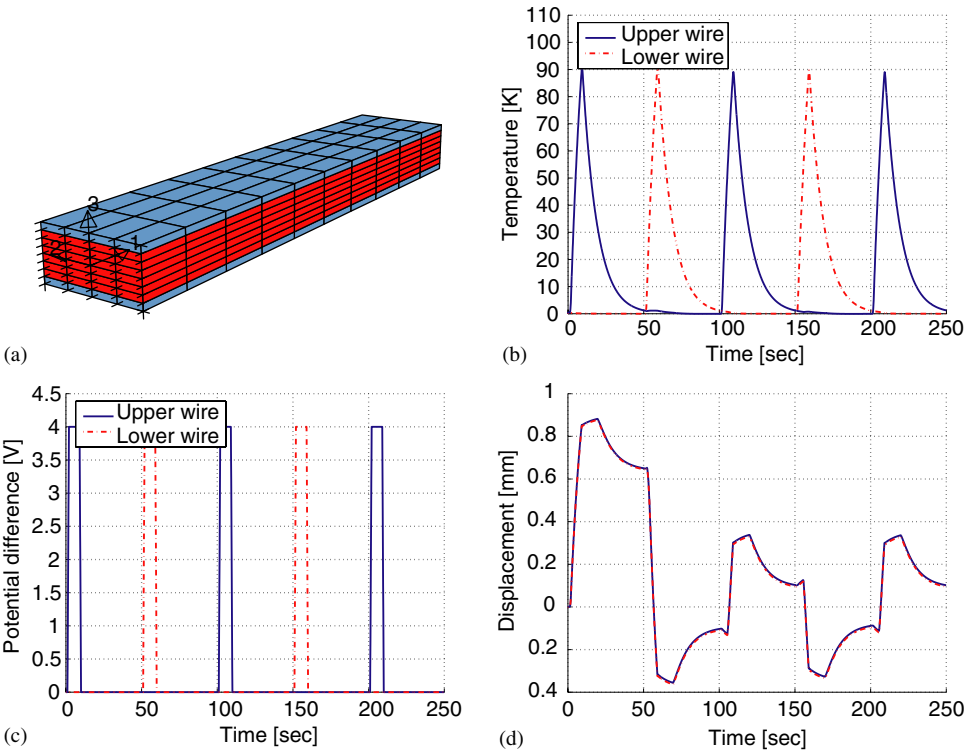

Figure 4. Model of hybrid composite with prestrained martensitic SMA wires (volume fraction $v_w = 0.125$) surface mounted on soft polymeric matrix (Problem B) (a). Active shape control by SMA wire actuated through Joule effect: temperature time history (b); potential difference time history (c); free edge displacement time history (d).

beam has a vertical displacement greater than 0.8 mm (Figures 4(d) and 5(a)). Successively, the beam temperature goes down to the room temperature by convection, the upper wire undergoes the reverse transformation from austenite to martensite and the beam shape changes finding an equilibrium configuration between the wire bending moment and the matrix resistant moment. Activating the lower wire, the cantilever goes back to the initial position and from here to a new position, bended in the opposite direction: in the studied case the tip of the beam has a vertical displacement of about -0.4 mm (Figures 4(d) and 5(b)). Also in this case, cooling the beam by convection a new configuration of equilibrium between the wire bending moment and the matrix resistant moment is found. Activating alternatively the two wires, the beam tip continuously goes up and down between ± 0.4 mm (Figures 4(d) and 5(c)–(d)). The right part of Figures 5 shows the axial stress changes induced in the composite after the first activation of the upper (a) and the lower (b) SMA wire and after the second activation of the upper (c) and the lower (d) SMA wire.

4.1.3. Problem C. We investigate the performance of the proposed computational tool in simulating the prestress induced by constrained strain recovery (*active stress control*). In particular,

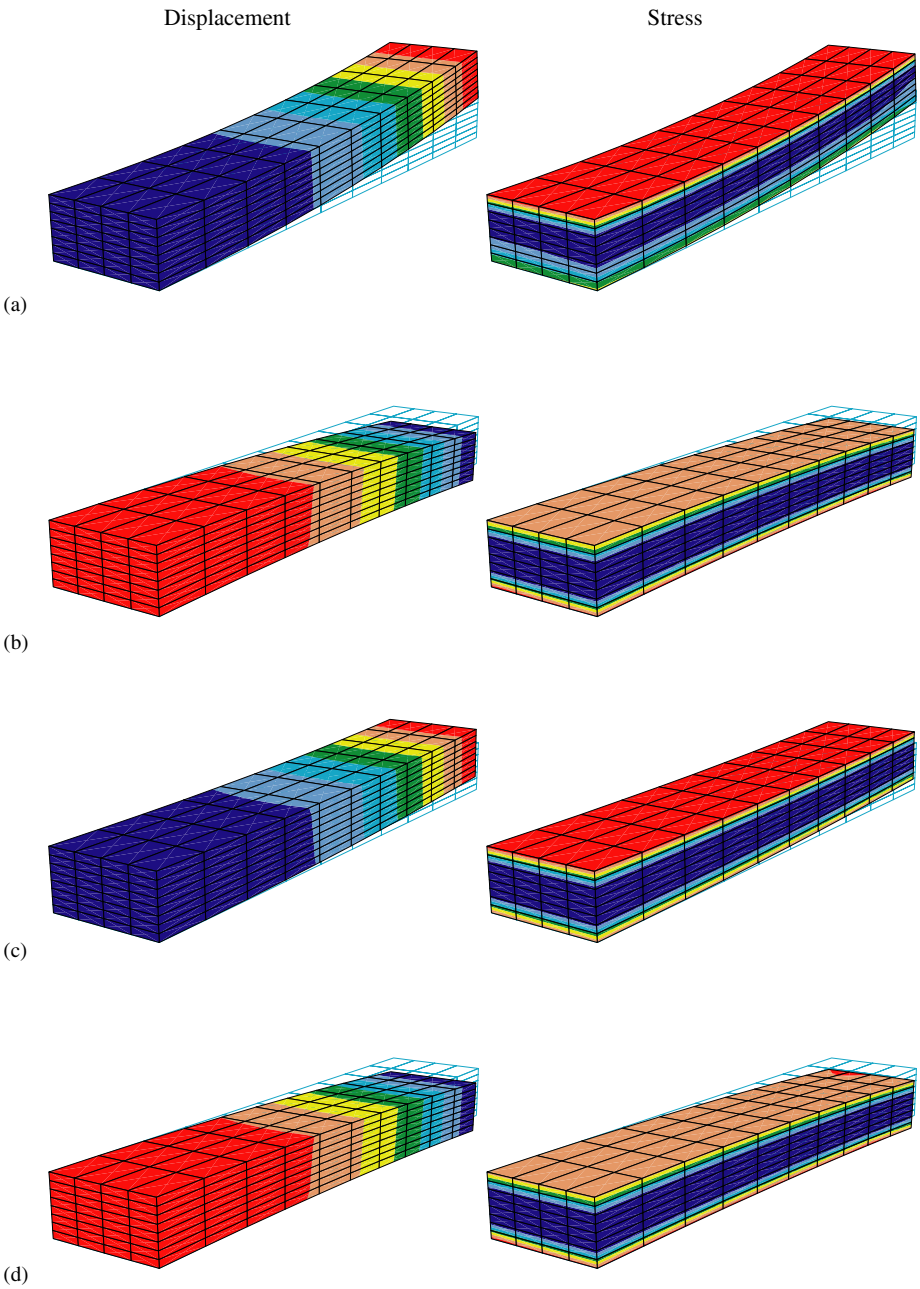

Figure 5. Problem B: vertical displacement (left part) and axial stress (right part) changes induced in the composite after the first activation of the upper (a) and the lower (b) SMA wire and after the second activation of the upper (c) and the lower (d) SMA wire.

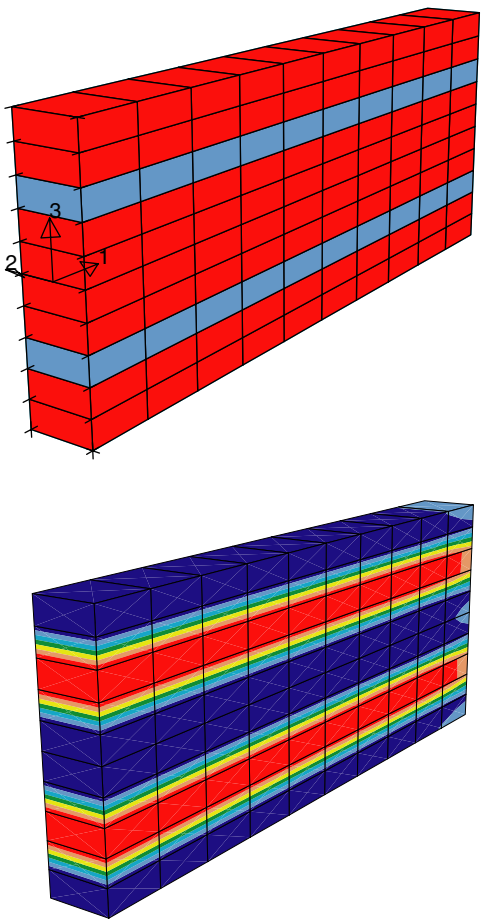

Figure 6. Model of hybrid composite with prestrained martensitic SMA wires (volume fraction $v_w = 0.2$) embedded in a stiff polymeric matrix (Problem C) (upper part). Prestress induced in the cantilever by SMA constrained strain recovery (lower part).

we consider a composite beam (dimension $10 \times 1 \times 4$ mm) with two Ni–Ti prestrained wires in martensitic phase, with volume fraction $v_w = 0.2$, embedded in a stiff polymeric matrix, along the x_1 direction (Figure 6 upper part). Room and body initial temperatures are set at $241\ \mathrm{K} = M_\mathrm{f}$.

SMA wires are simultaneously activated with the heat produced by Joule effect. Imposing a potential difference of 4 V at the edges of the wires, the wires heat above A_f and try to shrink. On the other hand, the polymeric matrix constrains the strain recovery and hence, while the wires experience tensile stresses, the matrix undergoes compressive stresses: in the studied case the compressive stresses reach the value of 400 MPa (Figure 6 lower part).

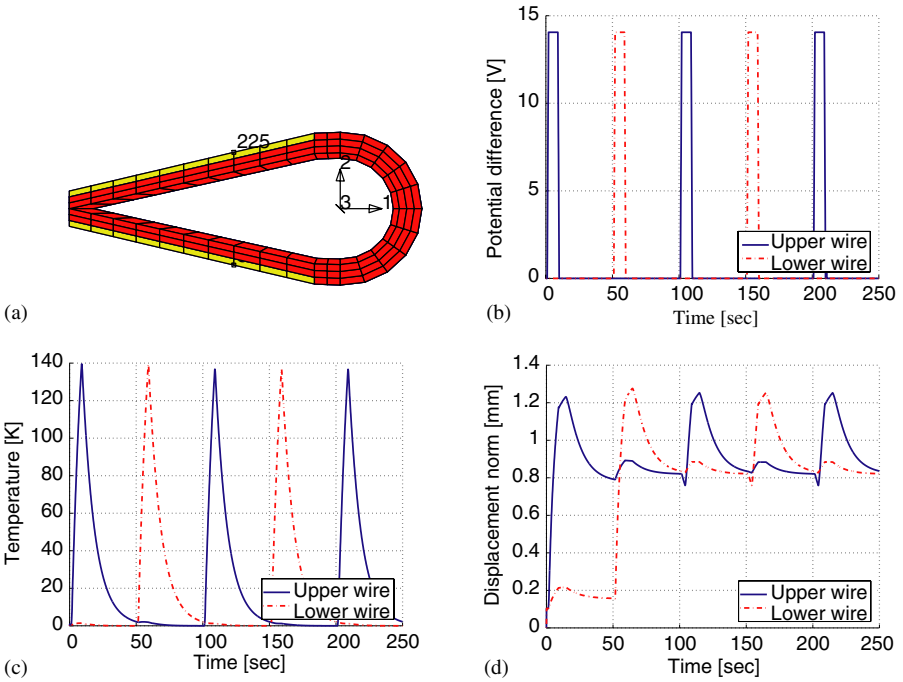

Figure 7. Model of an helicopter blade trailing edge flap (Problem D) (a). Active shape control by SMA wire actuated through Joule effect: potential difference time history of the two highlighted node (b); temperature time history of the two highlighted node (c); freeedge displacement time history of the two highlighted node (d).

4.1.4. Problem D. We investigate the performance of the proposed computational tool in simulating a peculiar promising application of SMA hybrid composite (*active blade flap control*): it has been shown [16] that helicopter blade vibration reduction is possible by trailing edge flap active control. Herein, we present a simplified model of an Aluminium flap with prestrained Ni–Ti fibres in martensitic phase surface mounted on. In particular we study a slice of the flap assuming plain strain conditions (Figure 7(a)).

As in Problem B, activating alternatively the upper and lower pre-strained SMA fibre, the flap shape can be actively controlled. Figure 7(b) shows the potential difference time variation of two points positioned in the central zone of the upper and lower wire as indicated in Figure 7(a). Figure 7(c)–(d) show the corresponding temperature and vertical displacement variations. Figure 8 shows the vertical displacement changes induced in the composite after the first activation of the upper (a) and the lower (b) SMA wire and after the second activation of the upper (c) and the lower (d) SMA wire.

5. CLOSURE AND FUTURE RESEARCH DIRECTIONS

We employ finite element method to study the behaviour of SMA hybrid composites: in particular, we develop a 3D solid finite element able to describe the thermo-electro-mechanical

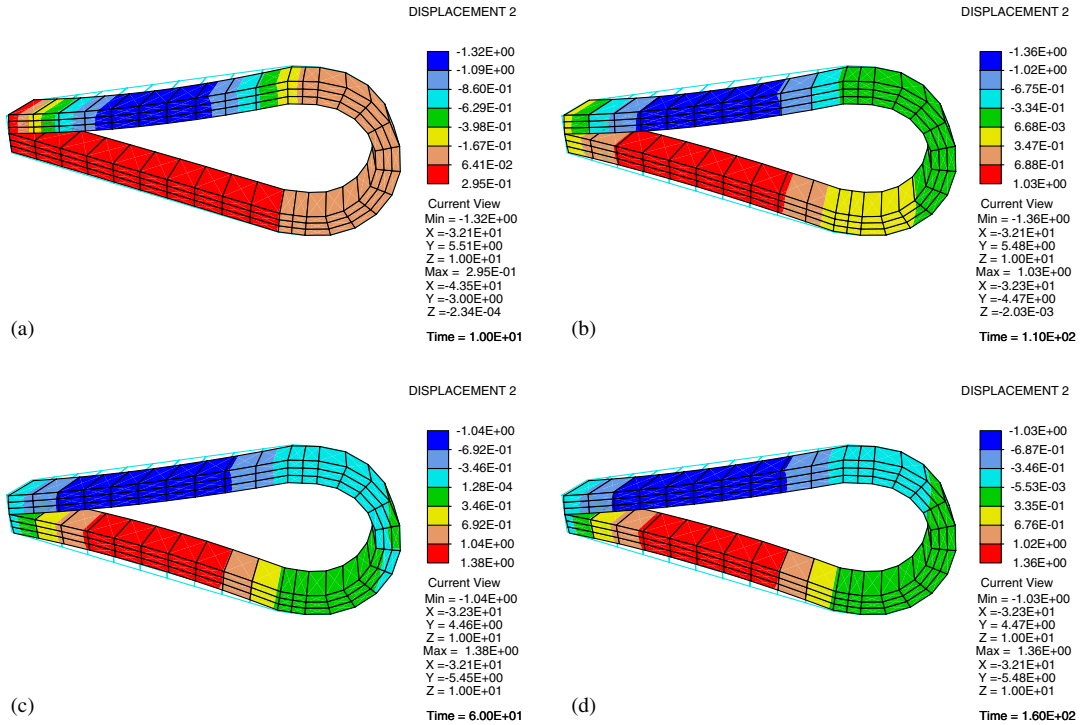

Figure 8. Problem D: vertical displacement changes induced in the composite after the first activation of the upper (a) and the lower (b) SMA wire and after the second activation of the upper (c) and the lower (d) SMA wire.

coupled problem due to shape memory alloy response and to Joule effect. Different feasible shape-memory-alloy composite applications are simulated.

The performed analyses show that the proposed computational tool is well suited for simulating SMA composite applications, giving interesting insights about the appliance responses.

Clearly, improvements are possible to capture other aspects, not considered here, such as delamination or sliding between matrix and wires. In particular, the object of further research will be to relax the assumption of isotropic elasto-plastic matrix as well as to introduce the SMA model capability of taking into account material parameter changes during martensitic transformation.

ACKNOWLEDGEMENTS

The present work has been partially developed within the joint French-Italian 'Lagrange laboratory' project as well as partially supported by the Ministero dell'istruzione, dell'università e della ricerca (MIUR) through the research program 'Shape-memory alloys: constitutive modeling, structural behaviour, experimental validation and applicability to innovative biomedical applications' and through the program of collaboration between CNR and MIUR (law 449/97).

We wish to thank Maria Rota (Università di Pavia) for her initial contribution to the work.

REFERENCES

1. van Moorleghem W, Besselink P, Aslanidis D (eds). *SMST-Europe 1999*, Antwerp Zoo, Belgium, 1999. CD-ROM only.
2. Russel SM, Pelton AR (eds). *Proceedings of the Third International Conference on Shape Memory and Superelastic Technologies*, Asilomar, CA, 2000.
3. Russel SM, Pelton AR (eds). *Proceedings of the Fourth International Conference on Shape Memory and Superelastic Technologies* Asilomar, CA, 2003.
4. Funakubo H. *Shape Memory Alloys*. Gordon and Breach: London, 1987 (Translated from the Japanese by J.B. Kennedy.).
5. Boller C, Brinson LC, Brand W, Huang MS. Some basic ideas on the design of adaptive aircraft structures using shape memory alloys. In *Proceedings of the 4th International Conference on Adaptive Structures*, Koln, 1993.
6. Guenin G, Guadez Ph. About the use of shape memory alloys in actuators. In *Proceedings of the Third International Conference on Intelligent Material*, Lyon, 1996.
7. Van Humbeeck J. On the adaptivity of shape memory alloys for use in adaptative materials. In *Proceedings of the Third International Conference on Intelligent Material*, Lyon, 1996.
8. Stalmans R, Michaud V, mBidaux J-E, Gotthardt R, Manson J-AE. Adaptative composites with embedded shape memory alloy wires. In *Proceedings of the 4th European Conference on Smart Structures and Materials*, Tomlinson GR, Bullough BWA (eds). Institute of Physics Publishing: Bristol, U.K. 1998.
9. Wei ZG, Sandstrom R, Miyazaki S. Shape memory materials and hybrid composites for smart systems. Part I: shape-memory materials. *Journal of Materials Science* 1998; **33**:3743–3762.
10. Reynaerts D, Van Brussel H. Design aspects of shape memory actuators. *Mechatronics* 1998; **8**:635–656.
11. Rogers CA. *Smart Materials*, *Structures*, *and Mathematical Issues*. Technomic: Lancaster, 1989.
12. Wei ZG, Sandstrom R, Miyazaki S. Shape memory materials and hybrid composites for smart systems. Part II: shape-memory hybrid composites. *Journal of Materials Science* 1998; **33**:3763–3783.
13. Schetky LMcD, Ming HWu. The properties and processing of shape memory alloys for use as actuators in intelligent composite materials. *Smart Structures and Materials* 1991; **24**:65–71.
14. Gaudenzi P, Mataluno S. On some applications of shape memory alloys to aerospace structures. In *Proceedings of the 4th International Conference on Adaptive Structures*, Koln, 1993.
15. Beauchamp CH, Nadolink RH, Dickinson SC, Dean LM. Shape memory alloy adjustable chamber (SMAAC) control surfaces. In *First European Conference on Smart Structures and Materials*, 1992; 189–192.
16. Song G, Kelly B, Agrawal BN. Active position control of a shape memory alloy wire actuated composite beam. *Smart Materials and Structures* 2000; **9**:711–716.
17. Barrett R, Gross RS. Super-active shape-memory alloy composites. *Smart Materials and Structures* 1996; **5**:255–260.
18. Wang G, Shahinpoor M. Design, prototyping and computer simulations of a novel large bending actuator made with a shape memory alloy contractile wire. *Smart Materials and Structures* 1997; **6**:214–221.
19. Maji AK, Negret I. Smart prestressing with shape memory alloy. *Journal of Engineering Mechanics* 1998; **124**:1121–1128.
20. Furuya Y. Design and material evaluation of shape memory composites. *Journal of Intelligent Material Systems and Structures* 1996; **7**:321–330.
21. Birman V, Chandrashekhara K, Sain S. Global strength of hybrid shape memory composite plates subjected to low velocity impact. *Journal of Reinforced Plastics and Composites* 1997; **16**:791–809.
22. Srinivasan AV, McFarland DM, Canistraro HA, Begg EK. Multiplexing embedded nitinol actuators to obtain increased bandwidth in structural control. *Journal of Intelligent Material Systems and Structures* 1997; **8**:202–214.
23. Ro J, Baz A. Nitinol-reinforced plates: part 3. Dynamic characteristics. *Composites Engineering* 1995; **5**:91–106.
24. Bidaux JE, Manson JAE, Gotthardt R. Active modification of the vibration frequencies of a polymer beam using shape-memory-alloy fibres. In *Proceedings of the Third International Conference on Intelligent Material*, Lyon, 1996.
25. Epps J, Chandra R. Shape memory alloy actuation for active tuning of composite beams. *Smart Materials and Structures* 1997; **6**:251–264.
26. Chen Q, Levy C. Vibration analysis and control of flexible beam by using smart damping structures. *Composites*: *Part B* 1999; **30**:395–406.

27. Venkatesh A, Hilborn J, Bidaux JE, Gotthardt R. Active vibration control of flexible linkage mechanisms using shape memory alloy fiber-reinforced composites. In *First European Conference on Smart Structures and Materials* 1992; 185–188.
28. Tsoi KA, Stalmans R, Schrooten J, Wevers M, Mai YM. Impact damage behavior of shape memory alloy composites. *Materials Science and Engineering A* 2003; **342**:207–215.
29. Paine JSN, Rogers CA. The response of SMA hybrid composite materials to low velocity impact. *Journal of Intelligent Material Systems and Structures* 1994; **5**:530–535.
30. Liang C, Rogers CA. Design of shape memory alloy actuators. *Journal of Intelligent Material Systems and Structures* 1997; **8**:303–313.
31. Seelecke S, Papenfuß N. A finite element formulation for SMA actuators. In *Proceedings of the 4th European Conference on Smart Structures and Materials*, Tomlinson GR, Bullough BWA (eds). Institute of Physics Publishing: Bristol, U.K., 1998.
32. Auricchio F, Petrini L. Improvements and algorithmical considerations on a recent three-dimensional model describing stress-induced solid phase transformations. *International Journal for Numerical Methods in Engineering* 2002; **55**:1255–1284.
33. Bidaux JE, Yu WJ, Gotthardt R, Manson JAE. Modelling of the martensitic transformation in shape memory alloy composites. *Journal de Physique IV*, *Colloque C2* 1995; **5**:543–548.
34. Auricchio F, Sacco E. Thermomechanical modelling of superelastic shape-memory alloy behavior. In *Computational Mechanics*: *New Trends and Applications*, *Proceedings of the Fourth World Congress on Computational Mechanics*, Idelsohn SR, Nate EO, Dvorkin EN (eds). Buenos Aires: Argentina, 1998.
35. Peyroux R, Chrysochoos A, Licht C, Lobel M. Thermomechanical couplings and pseudoelasticity of shape memory alloys. *International Journal of Engineering Science* 1998; **36**:489–509.
36. Bo Z, Lagoudas DC. Thermomechanical modeling of polycrystalline SMAs under cyclic loading, Part I: theoretical derivations. *International Journal of Engineering Science* 1999; **37**:1089–1140.
37. Lagoudas DC, Bo Z. Thermomechanical modeling of polycrystalline SMAs under cyclic loading, Part II: material characterization and experimental results from a stable transformation cycle. *International Journal of Engineering Science* 1999; **37**:1141–1173.
38. Bo Z, Lagoudas DC. Thermomechanical modeling of polycrystalline SMAs under cyclic loading, Part III: evolution of plastic strains and two-way shape memory effect. *International Journal of Engineering Science* 1999; **37**:1175–1203.
39. Bo Z, Lagoudas DC. Thermomechanical modeling of polycrystalline SMAs under cyclic loading, Part IV: modeling of minor hysteresis loops. *International Journal of Engineering Science* 1999; **37**:1205–1249.
40. Shaw JA. Simulations of localized thermo-mechanical behavior in a niti shape memory alloy. *International Journal of Plasticity* 2000; **16**:541–562.
41. Lim TJ, McDowell DL. Cyclic thermomechanical behavior of polycrystalline pseudoelastic shape memory alloy. *Journal of the Mechanics and Physics of Solids* 2002; **50**:651–676.
42. Auricchio F, Petrini L. A three-dimensional model describing stress-temperature induced solid phase transformations: solution algorithm and boundary value problems. *International Journal for Numerical Methods in Engineering*, 2004; accepted.
43. Leo PH, Shield TW, Bruno OP. Transient heat transfer effects on the pseudoelastic behavior of shape-memory wires. *Acta Metallurgica Materialia* 1993; **41**:2477–2485.
44. Chrysochoos A, Lobel M, Maisonneuve O. Thermomechanical coupling of pseudoelastic behaviour of CuZnAl and NiTi alloys. *Comptes Rendus de l'Academie des Sciences*, *Serie II* 1995; **320**:217–223.
45. Shaw JA, Kyriakides S. Thermomechanical aspects of NiTi. *Journal of the Mechanics and Physics of Solids* 1995; **43**:1243–1281.
46. Chrysochoos A, Pham H, Maissonneuve O. Energy balance of thermoelastic martensite transformation under stress. *Nuclear Engineering and Design* 1996; **162**:1–12.
47. Lim TJ, McDowell DL. Mechanical behavior of an Ni–Ti alloy under axial-torsional proportional and non-proportional loading. *Journal of Engineering Materials and Technology* 1999; **121**:9–18.
48. Lemaitre J, Chaboche JL. *Mechanics of Solid Materials*. Cambridge University Press: Cambridge, 1990.
49. Zienkiewicz OC, Taylor RL. *The Finite Element Method*, 5th edn, vol. I. Butterworth-Heinemann: New York, 2000.
50. Zienkiewicz OC, Taylor RL. *The Finite Element Method*, 5th edn, vol. II. Butterworth-Heinemann: New York, 2000.

51. Peyroux R, Chrysochoos A, Licht C, Lobel M. Phenomenological constitutive equations for numerical simulations of SMA's structures. Effects of thermomechanical couplings. *Journal de Physique IV* 1996; **C1-6**:347–356.
52. Zheng Y, Cui L, Li Y, Stalmans R. Partial transformation behavior of prestrained TiNi fibers in composites. *Materials Letters* 2001; **51**:425–428.
53. Zheng YJ, Schrooten J, Tsoi KA, Stalmans R. Thermal response of glass fibre/epoxy composites with embedded TiNiCu alloy wires. *Materials Science and Engineering A* 2002; **335**:157–163.
54. Vokoun D, Sittner P, Stalmans R. Study of the effect of curing treatment in fabrication of SMA/polymer composites on deformational behavior of NiTi-5at.% Cu SMA wires. *Scripta Materialia* 2003; **48**:623–627.
55. Thompson DM, Griffin Jr OH. Finite element predictions of active buckling control of stiffened panels. *Journal of Intelligent Material Systems and Structures* 1993; **4**:243–247.
56. Ro J, Baz A. Nitinol-reinforced plates: part 2. Static and buckling characteristics. *Composites Engineering* 1995; **5**:77–90.
57. Hurlbut BJ, Regelbrugge ME. Evaluation of a constitutive model for shape memory alloys embedded in shell structures. *Journal of Reinforced Plastics and Composites* 1996; **15**:1249–1261.
58. Benzaoui H, Lexcellent L, Chaillet N, Lang B, Bourjault A. Experimental study and modeling of a TiNi shape memory alloy wire actuator. *Journal of Intelligent Material Systems and Structures* 1997; **8**:619–629.
59. de Blonk BJ, Lagoudas DC. Actuation of elastomeric rods with embedded two-way shape memory alloy actuators. *Smart Materials and Structures* 1998; **7**:771–783.
60. Lagoudas DC, Bhattacharyya A. Modeling of thin layer extensional thermoelectric SMA actuators. *International Journal of Solids and Structures* 1998; **35**:331–362.
61. Ostachowicz W, Krawczuk M, Zak A. Natural frequencies of a multilayer composite plate with shape memory alloy wires. *Finite Elements in Analysis and Design* 1999; **32**:71–83.
62. Su Z, Mai H, Lu M, Ye L. Thermo-mechanical behaviour of shape memory alloy reinforced composite laminate (Ni–Ti/glass-fibre/epoxy). *Composite Structures* 1999; **47**:705–710.
63. Baz A, Chen T, Ro J. Shape control of NITINOL-reinforced beams. *Composites. Part B*: *Engineering* 2000; **31**:631–642.
64. Lau K-T, Zhou L-M, Tao X-M. Control of natural frequencies of a clamped-clamped composite beam with embedded shape memory alloy wires. *Composite Structures* 2002; **58**:39–47.
65. Aboudi J. The response of shape memory alloy composites. *Smart Materials and Structures* 1997; **6**:1–9.

